Springer

KSME

Journal of Mechanical Science and Technology 27 (7) (2013) 2093~2105
www.springerlink.com/content/1738-494x
DOI 10.1007/s12206-013-0528-6

Prediction of bend force and bend angle in air bending of electrogalvanized steel using response surface methodology †

R. Srinivasan[1,*], D. Vasudevan[2] and P. Padmanabhan[3]

[1]*RatnaVel Subramaniam College of Engineering and Technology, Dindigul, Tamilnadu, India*
[2]*PSNA College of Engineering and Technology, Dindigul, Tamilnadu, India*
[3]*VV College of Engineering , Tisaiyanvilai, Tamilnadu, India*

(Manuscript Received August 25, 2011; Revised January 2, 2013; Accepted March 19, 2013)

Abstract

This paper presents the development of predictive models for bend force and final bend angle (after springback) in air bending of electrogalvanized steel sheet employing response surface methodology. The models are developed based on five-level half factorial central composite design of experiments with strain hardening exponent, coating thickness, die opening, die radius, punch radius, punch travel, punch velocity as input parameters and bend force and final bend angle as responses. The results obtained from the models are in good accord with the experimental results. The effects of individual parameters and their interactions on the responses have also been analyzed in this study.

Keywords: Air bending; Bend force; Electrogalvanized steel; Final bend angle; Response surface methodology

1. Introduction

Bending is a widely used sheet metal forming process in the automobile industries. The process utilizes a press brake in which the sheet metal is bent into a die by a punch to produce bend component. Air bending technique [1] is used to improve the flexibility and efficiency of the bending process to meet out the higher accuracy and shorter lead time. In air bending, a number of different bend angles can be produced using the same set of tools simply by controlling the punch travel and hence there is a reduced need for tool changes.

Steel sheets are widely used to manufacture various components in the automotive industry. But the inherent weakness of steel parts is that they are susceptible to corrosion. Hence uncoated steel sheets are substituted with galvanized steel sheets because of their improved corrosion resistance. Galvanized steel sheets are manufactured either by hot dipping or by electrogalvanizing process. Since electrogalvanized (EG) steel sheets have better formability [2] and surface quality, it is much preferred than its counterpart hot dipped, for the applications including auto panels, hoods and gas tanks.

During the bending process, bend force is the force needed to deform the sheet metal to the required degree. When the punch is unloaded after completion of the bending process, elastic energy stored in sheet metal is released and the sheet metal tends to return to its initial state. The sheet returns to a final shape at which the residual stresses are in equilibrium. This effect is known as springback, and due to this the final bend angle after unloading (after springback) is changed from the initial bend angle before unloading. Very few studies on bend force and final bend angle are available in various bending processes. Huang and Leu [3] investigated the effect of process variables on punch load and final bend angle after unloading in closed die V bending process of steel sheet by performing experiments and finite element simulations. It was found that punch load increases as strain hardening exponent decreases and punch radius, punch speed increase. Moreover, the effects of process variables except bend radius on final bend angle are also limited. Hamouda et al. [4] studied the springback and load-displacement characteristics for different types of stainless steel in V bending process using finite element approach. They established that the bend force increases with increasing initial effective stress and coefficient of friction. Fei and Hodgson [5] did an experimental study to understand the springback and punch load behavior of TRIP steels in air V bending process. In this study, it was identified that the die gap and blank thickness have strong influence on the process. Narayanasamy and Padmanabhan [6, 7] presented experimental investigations on air bending process of interstitial free steel sheets to study important parameters affecting the springback and bend force. Garcia-Romeu and Ciurana [8]

*Corresponding author. Tel.: +91 9994277230, Fax.: +91 04551 227229
E-mail address: sriparam_2000@yahoo.com
† Recommended by Associate Editor Youngseog Lee

described the application of neural network techniques to air bending process for the prediction of springback and final bend angle. Farsi and Arezoo [9] developed a neural network model to predict the final bend angle for L-bending of perforated sheets. These investigations on bending show that the process parameters such as orientation, punch travel, punch radius, die opening, die radius and punch velocity have considerable influence on the bend force and final bend angle. The information on bend force provides a base to the designer for design of tooling and selection of press. The bend angle on unload has to be predicted accurately, thereby springback can be compensated by over-bending to obtain the desired bend angle [10]. In air bending, the bend force-punch travel relations are needed to achieve better in-process control**.** The potential application of bend angle-punch travel curves is to pre-set the press displacement in order to achieve the desired bend angle [11]. Hence, bend force and bend angle prediction is an essential practical issue and needs much attention in sheet metal bending.

Analytical approaches [11-15] for modeling the bending process are found in earlier literature. The major drawback with the analytical method is making simplifying assumptions, which limits the approach to simple geometries and deformation. Besides, it is difficult and cumbersome to develop an exact analytical model for bending process relating various parameters (material, tool and process) because of the complexity and constraints of the real process. An emerging approach to overcome this difficulty is to develop empirical-analytical models based on designed experiments and statistical techniques. Response surface methodology (RSM) is one such method which adopts mathematical and statistical techniques to evaluate the relation between a cluster of controlled experimental factors and a response. RSM is a well known method for process modeling and the method is well documented by Myers and Montgomery [16].

In recent years, RSM has been applied to model various metal forming processes. Kleiber, Knabel and Rojek [17] adopted RSM combined with finite element technique for probabilistic assessment of forming failures. Ohata et al. [18] developed a design system using RSM to find the annealing conditions suitable for sheet forming condition. Tiernan and Draganescu [19] described the application of RSM for modeling the extrusion force. Lepadatu et al. [20] developed an objective function using RSM for springback in L bending process considering die corner radius and clearance as input parameters, and did further optimization using FORTRAN gradient algorithm. Naceur, Guo and Ben-Elechi [21] employed RSM for optimization of tools geometry to reduce springback effects in sheet metal forming. Mkaddem and Saidene [22] applied RSM to develop prediction model for springback in wiping die bending process using three die radii, seven clearance values and two cut specimen directions. Bahloul, Ben-Elechi and Potiron [23] proposed an optimization methodology for springback of sheet metal in wiping die bending based on the use of experimental design and response surface techniques. From the literature, it is understood that RSM can be very well used for modeling sheet metal forming processes and in particular sheet metal bending. This paper presents the development of predictive models for bend force and final bend angle in air bending of electrogalvanized steel sheet employing response surface methodology.

2. Response surface methodology (RSM)

RSM provides an approximate relationship between the response Y and the input variables x_i which is based on the observed data from the process.

$$Y = f(x_1, x_2, x_3, ...x_n) + \varepsilon \tag{1}$$

where ε denotes an error component.

In general, the approximating function of the response Y is considered as second order polynomial, which is adequate. The second order model is represented by the following equation:

$$Y = \beta_0 + \sum_{i=1}^{k} \beta_i x_i + \sum_{i=1}^{k} \beta_{ii} x_i^2 + \sum_{i,j}^{k} \beta_{ij} x_i x_j + \varepsilon. \tag{2}$$

The response function Y at n data points can be written in matrix form as

$$Y = X\beta + \varepsilon, \tag{3}$$

$$Y = \begin{bmatrix} y_1 \\ y_2 \\ . \\ . \\ y_n \end{bmatrix}, \quad X = \begin{bmatrix} 1 & x_{11} & x_{12} & . & . & x_{1k} \\ 1 & x_{21} & x_{22} & . & . & x_{2k} \\ . & . & . & . & . & . \\ . & . & . & . & . & . \\ 1 & x_{n1} & x_{n2} & . & . & x_{nk} \end{bmatrix}$$

$$\beta = \begin{bmatrix} \beta_1 \\ \beta_2 \\ . \\ . \\ \beta_n \end{bmatrix} \text{ and } \varepsilon = \begin{bmatrix} \varepsilon_1 \\ \varepsilon_2 \\ . \\ . \\ \varepsilon_n \end{bmatrix}$$

where X is the matrix of model terms evaluated at n data points; β is the vector containing unknown coefficients; ε is the error vector.

The unbiased b of the coefficient vector β is obtained by using the least square error method as:

$$b = \left(X^T X\right)^{-1} X^T Y. \tag{4}$$

By obtaining coefficient vector b from Eq. (4), the response surface is prepared.

- Identifying the important process parameters that influencing the response and choosing their upper and lower limits.
- Developing an experimental design matrix.

- Conducting the experiments as per the design matrix and recording the responses.
- Calculating the coefficients of the polynomials.
- Checking the significance of coefficients and arriving at final mathematical model.
- Checking the adequacy of the model.
- Conducting the confirmation experiments
- Analyzing the effect of process parameters on response.

In this investigation, MINITAB 15 software has been used for the development of the RSM model.

2.1 Identification of process parameters and choosing their limits

A literature survey [3-10] has been performed to identify the process parameters influencing the bend force and final bend angle. Seven independently controllable process parameters namely, strain hardening exponent (*n)*, coating thickness (t_c), die opening (W_d), die radius (R_d), punch radius (R_p) , punch travel (t_p) and punch velocity (V_p) were identified as important parameters influencing the bend force and final bend angle.

It is often convenient to use the coded value of a design variable. The upper level of a variable is coded as +2.82 and the lower level as -2.82 for designing the experiments. The intermediate coded values of design variable are obtained from the equation as follows.

$$\text{Coded value of the parameter value } \varsigma_i = \frac{x_i - x_{i0}}{d_i} \quad (5)$$

where x_i is the actual parameter value, x_{i0} is the parameter value corresponding to zero level and d_i is the incremental parameter value. The actual and coded values of the process parameters are listed in Table 1.

2.2 Developing the experimental design matrix

The experimental design matrix chosen was seven factor, five level, half factorial central composite rotatable design (CCRD). The design consists of half replication of 2^7 (128/2 = 64) design points plus 10 center points and 14 star points, which is shown in Table 2. The process variables at their intermediate level (0) constitute the center points, and the combination of each of the variables at its lowest (-2.82) or highest (+2.82) with the other factors at their intermediate level constitutes the star points. This 88 experimental runs establish the mathematical relation of the response surface models for bend force and final bend angle by estimating the linear, quadratic and interactive terms of the process variables.

2.3 Conducting the experiments and recording the responses

The blanks from the coated and uncoated steel sheets were cut to the required dimensions of 120 mm X 40 mm X 1 mm and the edges were cleaned to remove the burrs. As the strain-hardening exponent *n* values (0.211, 0.219, 0.232, 0.206 and 0.227) belong to five different orientations 0°, 22.5°, 45°, 67.5° and 90°, respectively, the blanks were prepared in the five directions. A 40 ton universal testing machine (UTM) was used for conducting the air bending experiments. The tool set consists of a die and a punch, made of hardened steel. The tooling setup for the experiments is shown in Fig. 1. In UTM, the punch was mounted in the cross head and the die was located on the platform. The blanks were placed on the die in proper position with necessary care. The steel blanks were bent by moving the punch gradually to the required depth. The corresponding punch travel and the bend force were measured from the digital display of UTM and the load cell setup, respectively. The bend force values were converted for unit meter width as it is a common unit found in bend force charts. The longer edge of the bent sample was coated with black ink, and the impression of the profile was taken carefully on a thick white paper supported by a board. The impressions of the sheet were scanned and converted into digitized images. The digitized images were imported to CAD software, and the lines were drawn on the edges of the legs of the images using software. The necessary angles were measured using CAD software [24]. The experiments were conducted as per the design matrix at random to avoid systematic errors and the response values (bend force and final bend angle) were recorded. The experimental design matrix along with the experimental results of responses is given in Table 2.

Table 1. Scheme of levels and values of parameters.

Parameters	Parameter levels				
	-2.82	**-1**	**0**	**+1**	**+2.82**
Strain hardening exponent (*n*)	0.206	0.211	0.219	0.227	0.232
Coating thickness (t_c) μm	0	4	7	10	14
Die opening (W_d) in mm	40	55	60	65	80
Die radius (R_d) in mm	3	5	6.5	8	10
Punch radius (R_p) in mm	4	8	10	12	16
Punch travel (t_p) in mm	5	12	15	18	25
Punch velocity (V_p) in mm/s	0.2	0.45	0.6	0.75	1

2.4 Estimating the coefficients of models and their significance

The experimental data were analyzed to obtain the coefficients of polynomials using MINITAB software. The *p* value approach is used for testing the significance of coefficients. According to this, the coefficients are tested at the 0.05 level of significance (95% confidence level). The coefficients which have *p* value less than 0.05 are considered as significant.

The coefficients and *p* values from the analysis for bend force are listed in Table 3. It is found that the coefficients of t_c,

Table 2. Design matrix and experimental results of responses.

Expt. No	Design parameters							Experimental results	
	Strain hardening exponent (n)	Coating thickness (t_c) μm	Die opening (W_d) mm	Die radius (R_d) mm	Punch radius (R_p) mm	Punch travel (t_p) mm	Punch velocity (V_p) mm/s	Bend Force (Y_1) kN/m	Final Bend Angle (Y_2) Deg
1	0.211	4	55	5.0	8	12	0.75	4.60	49.54
2	0.227	4	55	5.0	8	12	0.45	4.81	48.62
3	0.211	10	55	5.0	8	12	0.45	4.38	51.51
4	0.227	10	55	5.0	8	12	0.75	4.08	55.81
5	0.211	4	65	5.0	8	12	0.45	3.96	40.01
6	0.227	4	65	5.0	8	12	0.75	3.61	44.51
7	0.211	10	65	5.0	8	12	0.75	3.27	47.62
8	0.227	10	65	5.0	8	12	0.45	3.32	47.25
9	0.211	4	55	8.0	8	12	0.45	4.59	44.45
10	0.227	4	55	8.0	8	12	0.75	4.36	48.70
11	0.211	10	55	8.0	8	12	0.75	3.89	51.33
12	0.227	10	55	8.0	8	12	0.45	3.98	51.06
13	0.211	4	65	8.0	8	12	0.75	3.49	40.13
14	0.227	4	65	8.0	8	12	0.45	3.68	40.10
15	0.211	10	65	8.0	8	12	0.45	3.21	42.89
16	0.227	10	65	8.0	8	12	0.75	2.89	47.16
17	0.211	4	55	5.0	12	12	0.45	5.07	49.73
18	0.227	4	55	5.0	12	12	0.75	4.79	54.22
19	0.211	10	55	5.0	12	12	0.75	4.38	56.33
20	0.227	10	55	5.0	12	12	0.45	4.48	55.11
21	0.211	4	65	5.0	12	12	0.75	3.87	45.62
22	0.227	4	65	5.0	12	12	0.45	4.02	44.47
23	0.211	10	65	5.0	12	12	0.45	3.67	46.84
24	0.227	10	65	5.0	12	12	0.75	3.30	51.36
25	0.211	4	55	8.0	12	12	0.75	4.57	49.74
26	0.227	4	55	8.0	12	12	0.45	4.85	48.82
27	0.211	10	55	8.0	12	12	0.45	4.29	50.59
28	0.227	10	55	8.0	12	12	0.75	4.00	54.86
29	0.211	4	65	8.0	12	12	0.45	3.91	40.20
30	0.227	4	65	8.0	12	12	0.75	3.66	44.70
31	0.211	10	65	8.0	12	12	0.75	3.19	46.70
32	0.227	10	65	8.0	12	12	0.45	3.20	46.30
33	0.211	4	55	5.0	8	18	0.45	4.69	69.34
34	0.227	4	55	5.0	8	18	0.75	4.24	73.95
35	0.211	10	55	5.0	8	18	0.75	3.89	75.85
36	0.227	10	55	5.0	8	18	0.45	4.05	75.53
37	0.211	4	65	5.0	8	18	0.75	3.65	62.33
38	0.227	4	65	5.0	8	18	0.45	3.81	62.22
39	0.211	10	65	5.0	8	18	0.45	3.47	64.33
40	0.227	10	65	5.0	8	18	0.75	3.03	68.82
41	0.211	4	55	8.0	8	18	0.75	4.19	69.31
42	0.227	4	55	8.0	8	18	0.45	4.37	69.31
43	0.211	10	55	8.0	8	18	0.45	3.92	70.83
44	0.227	10	55	8.0	8	18	0.75	3.55	75.18
45	0.211	4	65	8.0	8	18	0.45	3.78	57.69
46	0.227	4	65	8.0	8	18	0.75	3.38	62.28
47	0.211	10	65	8.0	8	18	0.75	2.95	64.01
48	0.227	10	65	8.0	8	18	0.45	3.08	65.04
49	0.211	4	55	5.0	12	18	0.75	4.82	75.06
50	0.227	4	55	5.0	12	18	0.45	5.10	74.05
51	0.211	10	55	5.0	12	18	0.45	4.65	74.99
52	0.227	10	55	5.0	12	18	0.75	4.26	79.46
53	0.211	4	65	5.0	12	18	0.45	4.40	62.40
54	0.227	4	65	5.0	12	18	0.75	3.97	67.13
55	0.211	10	65	5.0	12	18	0.75	3.64	68.27
56	0.227	10	65	5.0	12	18	0.45	3.71	67.77
57	0.211	4	55	8.0	12	18	0.45	4.95	69.39
58	0.227	4	55	8.0	12	18	0.75	4.61	73.97
59	0.211	10	55	8.0	12	18	0.75	4.12	74.59
60	0.227	10	55	8.0	12	18	0.45	4.28	74.19
61	0.211	4	65	8.0	12	18	0.75	3.90	62.38
62	0.227	4	65	8.0	12	18	0.45	4.16	62.25
63	0.211	10	65	8.0	12	18	0.45	3.66	63.06
64	0.227	10	65	8.0	12	18	0.75	3.28	67.47
65	0.206	7	60	6.5	10	15	0.6	3.98	57.00
66	0.232	7	60	6.5	10	15	0.6	3.85	60.07
67	0.219	0	60	6.5	10	15	0.6	4.75	53.28
68	0.219	14	60	6.5	10	15	0.6	3.59	62.46
69	0.219	7	40	6.5	10	15	0.6	6.29	79.03
70	0.219	7	80	6.5	10	15	0.6	2.88	47.51
71	0.219	7	60	3.0	10	15	0.6	4.16	61.44
72	0.219	7	60	10.0	10	15	0.6	3.63	55.33
73	0.219	7	60	6.5	4	15	0.6	3.42	55.46
74	0.219	7	60	6.5	16	15	0.6	4.36	61.44
75	0.219	7	60	6.5	10	5	0.6	3.38	20.54
76	0.219	7	60	6.5	10	25	0.6	3.34	89.85
77	0.219	7	60	6.5	10	15	0.2	4.23	55.15
78	0.219	7	60	6.5	10	15	1	3.53	61.89
79	0.219	7	60	6.5	10	15	0.6	3.84	58.43
80	0.219	7	60	6.5	10	15	0.6	3.84	58.43
81	0.219	7	60	6.5	10	15	0.6	3.84	58.42
82	0.219	7	60	6.5	10	15	0.6	3.84	58.43
83	0.219	7	60	6.5	10	15	0.6	3.84	58.43
84	0.219	7	60	6.5	10	15	0.6	3.84	58.44
85	0.219	7	60	6.5	10	15	0.6	3.84	58.43
86	0.219	7	60	6.5	10	15	0.6	3.84	58.42
87	0.219	7	60	6.5	10	15	0.6	3.84	58.43
88	0.219	7	60	6.5	10	15	0.6	3.84	58.43

Table 3. Terms, coefficients and their p values for bend force (Before elimination).

Term	Coefficient	p value	Term	Coefficient	P value
Constant	52.641	0.000	nxR_p*	0.244	0.149
n	-304.491	0.000	nxt_p	-0.312	0.007
t_c*	0.020	0.486	nxV_p*	4.036	0.075
W_d	-0.294	0.000	$t_c xW_d$*	0.000	0.727
R_d	-0.379	0.000	t_cxR_d	-0.004	0.000
R_p	-0.109	0.013	t_cxR_p*	-0.001	0.117
t_p	-0.082	0.005	t_cxt_p*	-0.000	0.224
V_p	-2.053	0.001	t_cxV_p	0.026	0.000
nxn	721.323	0.000	W_dxR_d	0.001	0.004
t_cxt_c	0.007	0.000	W_dxR_p	-0.001	0.000
W_dxW_d	0.002	0.000	W_dxt_p	0.003	0.000
R_dxR_d	0.006	0.000	W_dxV_p*	0.004	0.324
R_pxR_p	0.002	0.000	R_dxR_p*	0.000	0.727
t_pxt_p	-0.005	0.000	R_dxt_p	0.002	0.000
V_pxV_p	0.310	0.003	R_dxV_p*	0.022	0.069
nxt_c	-0.671	0.000	R_pxt_p	0.011	0.000
nxW_d	-0.289	0.000	R_pxV_p*	-0.001	0.916
nxR_d	0.664	0.004	t_pxV_p	-0.039	0.000

* Insignificant terms

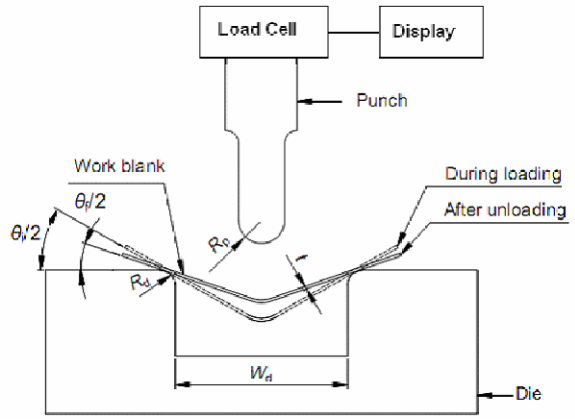

Fig. 1. Experimental setup.

R_p: punch radius; R_d: die radius; W_d: die opening; t: sheet thickness; θ_i: bend angle (during loading); θ_f: bend angle (after unloading)

nxR_p, nxV_p, t_cxW_d, t_cxR_p, t_cxt_p, W_dxV_p, R_dxR_p, R_dxV_p and R_pxV_p are insignificant. These insignificant terms except t_c can be removed by using backward elimination process [25].The model building principle suggests that when a particular polynomial term is included in a model, all lower order polynomial terms should also be included to preserve the hierarchy [26] . Hence when the higher order square term t_c^2 is included in the model, the lower order linear term t_c is also included to preserve the hierarchy in the model.

The backward elimination process to adjust the model eliminates the insignificant terms, and the coefficients and p values after elimination are presented in Table 4. The results from the table reveal that the terms are significant as the p values are less than 0.05.

Table 4. Terms, coefficients and their p values for bend force (After elimination).

Term	Coefficient	p value	Term	Coefficient	p value
Constant	51.410	0.000	nxt_c	-0.671	0.000
n	-299.629	0.000	nxW_d	-0.289	0.000
t_c	-0.029	0.283	nxR_d	0.664	0.006
W_d	-0.291	0.000	nxt_p	-0.312	0.009
R_d	-0.363	0.000	t_cxR_d	-0.004	0.000
R_p	-0.059	0.005	t_cxV_p	0.026	0.000
t_p	-0.085	0.005	W_dxR_d	0.001	0.005
V_p	-0.823	0.000	W_dxR_p	-0.001	0.005
nxn	721.323	0.000	W_dxt_p	0.003	0.000
t_cxt_c	0.007	0.000	R_dxt_p	0.002	0.001
W_dxW_d	0.002	0.000	R_pxt_p	0.011	0.000
R_dxR_d	0.006	0.000	t_pxV_p	-0.039	0.000
R_pxR_p	0.002	0.001			
t_pxt_p	-0.005	0.000			
V_pxV_p	0.310	0.004			

Table 5. Terms, coefficients and their p values for final bend angle (Before elimination).

Term	Coefficient	p value	Term	Coefficient	p value
Constant	70.843	0.000	nxR_p	-4.036	0.000
n	-379.987	0.001	nxt_p	3.234	0.000
t_c	1.151	0.000	nxV_p	-39.225	0.000
W_d	-1.933	0.000	t_cxW_d	0.008	0.000
R_d	-1.821	0.000	t_cxR_d	-0.006	0.004
R_p	2.308	0.000	t_cxR_p	-0.047	0.000
t_p	6.738	0.000	t_cxt_p	-0.022	0.000
V_p	21.087	0.000	t_cxV_p	-0.006	0.000
nxn	892.722	0.001	W_dxR_d	0.009	0.000
t_cxt_c	-0.011	0.008	W_dxR_p	-0.007	0.000
W_dxW_d	0.012	0.000	W_dxt_p	-0.045	0.000
R_dxR_d*	-0.002	0.686	W_dxV_p	-0.056	0.000
R_pxR_p*	0.001	0.514	R_dxR_p	-0.030	0.000
t_pxt_p	-0.032	0.000	R_dxt_p*	0.001	0.686
V_pxV_p	0.693	0.050	R_dxV_p	-0.373	0.000
nxt_c*	0.457	0.245	R_pxt_p	-0.012	0.000
nxW_d	1.606	0.000	R_pxV_p	0.279	0.000
nxR_d	4.671	0.000	t_pxV_p	-0.093	0.000

* Insignificant terms

The coefficients and p values from the analysis for bend angle are listed in Table 5. It is found that the coefficients of R_dxR_d, R_pxR_p, nxt_c, and R_dxt_p are insignificant. These insignificant terms are removed by using backward elimination process, and after elimination the coefficients and p values are presented in Table 6. The results show that the terms are significant.

Table 6. Terms, coefficients and their p values for final bend angle (After elimination).

Term	Coefficient	p value	Term	Coefficient	p value
Constant	69.502	0.000	nxt_p	3.234	0.000
n	-372.300	0.001	nxV_p	-39.225	0.000
t_c	1.251	0.000	$t_c xW_d$	0.008	0.000
W_d	-1.933	0.000	$t_c xR_d$	-0.006	0.003
R_d	-1.831	0.000	$t_c xR_p$	-0.047	0.000
R_p	2.330	0.000	$t_c xt_p$	-0.022	0.000
t_p	6.744	0.000	$t_c xV_p$	-0.106	0.000
V_p	21.102	0.000	$W_d xR_d$	0.009	0.000
nxn	882.480	0.001	$W_d xR_p$	-0.007	0.000
$t_c xt_c$	-0.011	0.000	$W_d xt_p$	-0.045	0.000
$W_d xW_d$	0.012	0.000	$W_d xV_p$	-0.056	0.000
$t_p xt_p$	-0.032	0.000	$R_d xR_p$	-0.030	0.000
$V_p xV_p$	0.681	0.049	$R_d xV_p$	-0.373	0.000
nxW_d	1.606	0.000	$R_p xt_p$	-0.012	0.000
nxR_d	4.671	0.000	$R_p xV_p$	0.279	0.000
nxR_p	-4.036	0.000	$t_p xV_p$	-0.093	0.000

2.5 Developed final model

The final mathematical models for bend force and final bend angle are obtained through the backward elimination process and are given in terms of factors, as follows.

Bend force,

$$\begin{aligned} Y_1 &= 51.410 - 299.629n - 0.029t_c - 0.0291W_d - 0.363R_d \\ &-0.059R_p - 0.085t_p - 0.823V_p + 721.323n^2 + 0.007t_c^2 \\ &+0.002W_d^2 + 0.006R_d^2 - 0.005t_p^2 + 0.310V_p^2 - 0.671nt_c \\ &-0.289nW_d + 0.664nR_d - 0.312nt_p - 0.004t_cR_d \\ &+0.026t_cV_p + 0.001W_dR_d - 0.001W_dR_p + 0.003W_dt_p \\ &+0.002R_dt_p + 0.011R_pt_p - 0.039t_pV_p \end{aligned} \quad (6)$$

where n is the strain hardening exponent, t_c is the coating thickness, W_d is the opening, R_d is the die radius, R_p is the punch radius, t_p is the punch travel and V_p is the punch velocity.

Final bend angle,

$$\begin{aligned} Y_2 &= 69.502 - 372.300n + 1.251t_c - 1.933W_d - 1.831R_d \\ &+2.220R_p + 6.744t_p + 21.102V_p + 882.480n^2 \\ &-0.011t_c^2 + 0.012W_d^2 - 0.032t_p^2 + 0.681V_p^2 + 1.606nW_d \\ &+4.671nR_d - 4.036nR_p + 3.234nt_p - 39.225nV_p \\ &+0.008t_cW_d - 0.006t_cR_d - 0.047t_cR_p - 0.022t_ct_p \\ &-0.106t_cV_p + 0.009W_dR_d - 0.007W_dR_p - 0.056W_dV_p \\ &-0.03R_dR_p - 0.373R_dV_p - 0.012R_pt_p + 0.279R_pV_p \\ &-0.093t_pV_p. \end{aligned} \quad (7)$$

Table 7. ANOVA table for the bend force model.

Source	DF	Seq SS	Adj SS	Adj MS	F	P
Regression	26	28.8899	28.8899	1.111151	2249.32	0.0
Linear	7	26.5638	0.19683	0.028118	56.92	0.0
Square	7	1.7903	1.79033	0.255762	517.74	0.0
Interaction	12	0.5357	0.53574	0.044645	90.38	0.0
Residual error	61	0.0301	0.03013	0.000494		
Lack of fit	52	0.0301	0.03013	0.000579	1.174	
Pure error	9	0.00444	0.00444	0.000493		
R^2 0.999		R^2 adjusted 0.9985		R^2 predicted 0.9971		

F ratio = MS of Lack-of-Fit/ MS of error
F estimated = 1.174; Standard value F (0.05, 52, 9) = 2.797

Table 8. ANOVA table for the final bend angle model.

Source	DF	Seq SS	Adj SS	Adj MS	F	P
Regression	31	11618.9	11618.9	374.804	69537.8	0.0
Linear	7	11509.1	41.7329	5.9618	1106.11	0.0
Square	5	68.4	68.4017	13.6803	2538.13	0.0
Interaction	19	41.4	41.3996	2.1789	404.26	0.0
Residual error	56	0.3	0.3018	0.0054		
Lack of fit	47	0.3	0.3016	0.0064	1.187	
Pure error	9	0.04850	0.0485091	0.005389		
R^2 0.999		R^2 adjusted 0.9995		R^2 predicted 0.9995		

F ratio = MS of Lack-of-Fit/ MS of error
F estimated = 1.187; Standard value F (0.05, 47, 9) = 2.806

2.6 Checking the adequacy of the developed models

The analysis of variance (ANOVA) for the developed models was calculated with the help of MINITAB (Version 15) software and the results are presented in Tables 7 and 8 The adequacy test of the developed mathematical model was performed by Fisher's variance ratio test known as F test. As per this test, the calculated value of F ratio for the lack-of-fit must be lesser than its standard table value for a desired level of confidence level. Since the estimated F value (1.174) is lesser than the table value (2.797) for bend force model, it is assured that the model is adequate at a confidence level of 95%. In the case of final bend angle model, as the estimated F value (1.187) is lesser than the standard table value (2.806), it is certain that the final bend angle model is adequate at a confidence level of 95%. Further, the regression statistics values R^2 and R^2_{adj} values are 0.999 and 0.9985, respectively, for bend force model and the values are 0.999 and 0.9995, respectively, for final bend angle model. The R^2 value is high and close to 1 and it is in close agreement with the R^2_{adj}, which is desirable.

The adequacies of the models have also been further supported by the examination of residuals. The normal probability plot of the residuals should form a straight line [25], and the plot of the residuals versus the fitted values should not have an

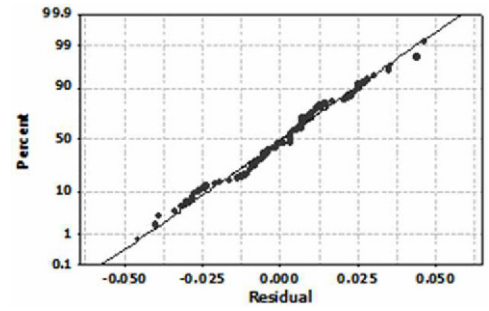

(a)

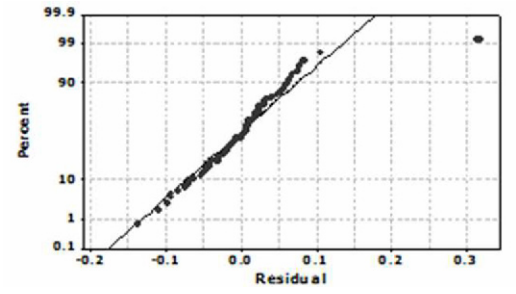

(b)

Fig. 2. Normal probability plot of residuals: (a) Bend force; (b) Final bend angle.

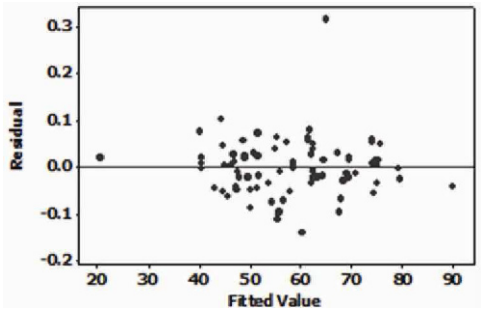

(a)

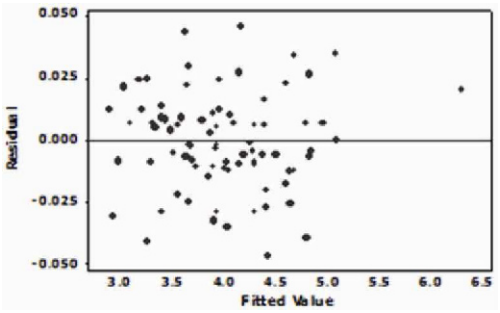

(b)

Fig. 3. Plot of the residuals versus the fitted value: (a) Bend force; (b) Final bend angle.

obvious pattern [27] if the model is adequate. The normal probability plots of the residuals and the plots of the residuals versus the fitted values are shown in Figs. 2(a), 2(b), 3(a), 3(b). From Figs. 2(a), 2(b), the residuals fall on a straight line, indicating that the errors are distributed normally. There is no obvious pattern in the plot of the residuals versus fitted value shown in Figs. 3(a) and 3(b), which models proposed are adequate. Hence, the predictive models given in Eqs. (6) and (7) are adequate and could be used for predicting the bend force and final bend angle respectively.

Table 9. Comparison of experimental and predicted values of responses.

Response	(n)	(t_c)μm	(W_d) mm	(R_d)mm	(R_p)mm	(t_p)mm	(V_p)mm/s	Experimental(Y_{exp})	Predi-cted (Y_p)	Error %
Bend force	0.211	4	60	5	8	10	0.4	4.42	4.62	4.58
	0.227	7	80	3	16	15	0.6	3.89	4.01	3.18
	0.232	10	40	8	12	20	0.8	5.38	5.60	4.1
Bend angle	0.211	4	60	5	8	10	0.4	33.45	34.48	3.07
	0.227	7	80	3	16	15	0.6	51.75	52.55	1.54
	0.232	10	40	8	12	20	0.8	101.52	103.3	1.74

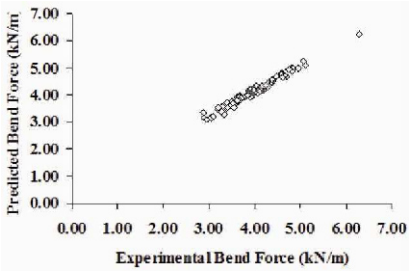

(a)

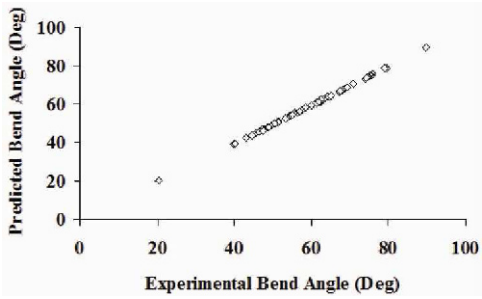

(b)

Fig. 4. Scatter diagram: (a) Bend force; (b) Final bend angle.

2.7 Conducting the confirmation experiments

The validity of the model is further tested by drawing a scatter diagram as shown in Figs. 4(a) and 4(b), which indicates the correlation between the experimental values and predicted values of bend force and final bend angle. There is a good correlation between the experimental and model results. Confirmation experiments were also conducted for intermediate values of the process variables and the results were com-

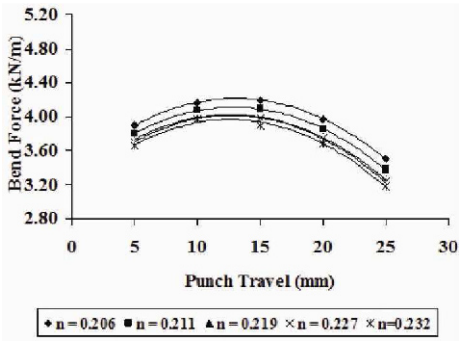

(a)

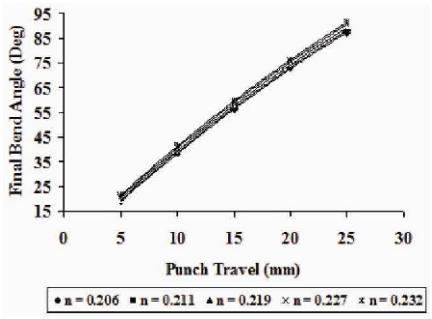

(b)

Fig. 5. Effect of strain hardening exponent on (a) Bend force; (b) Final bend angle (t_c = 7μ, W_d = 60 mm , R_d = 6.5 mm, R_p =10 mm, V_p = 0.6 mm/s).

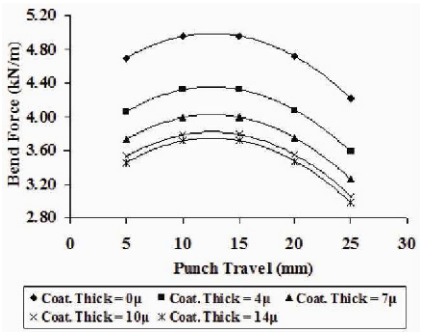

(a)

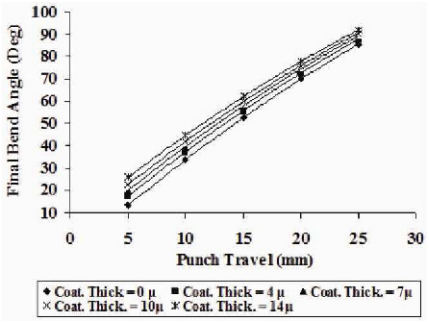

(b)

Fig. 6. Effect of coating thickness on (a) Bend force; (b) Final bend angle (n = 0.219, W_d = 60 mm, R_d = 6.5 mm, R_p =10 mm, V_p = 0.6 mm/s).

pared with the results of prediction models. The process parameters used in the confirmation experiments and the comparison between experimental and predicted values are shown in Table 9. The error was calculated by the equation as follows:

$$Error(\%) = \left| \frac{(Y_p - Y_{\exp})}{Y_{\exp}} \right| \times 100 \quad (8)$$

where Y_p is the predicted value and Y_{exp} is the experimental value**.** It is observed from the comparison table that the predicted values from the models are in good accord with the experimental values.

3. Results and discussion

This section discusses the direct and few important interaction effects of process parameters.

3.1 Direct effects of process parameters on bend force and final bend angle

The direct effects of process parameters on bend force and final bend angle are illustrated with bend force - punch travel and final bend angle - punch travel curves for different parameters as shown in Figs. 5-10. The graphs are drawn by varying the parameter whose effect is to be analyzed at all five levels and considering the other parameters at 0 - level.

The influence of punch travel on bend force and bend angle can be understood from Figs. 5-10. The bend force increases with the punch travel and reaches a maximum value and then gradually falls. This increase in bend force is caused by the development and spreading of plastic zone [28]. This fall in bend force results from the lower deformation resistance and large rigid body displacement [4]. As the sheet is more deformed with the increase in punch travel, the bend angle increases continuously.

The effect of strain hardening on bend force and bend angle is shown in Figs. 5(a) and 5(b). The bend force decreases with increase of strain hardening exponent. Strain hardening exponent (n) represents the ability of the metal to undergo plastic deformation [29] and hence bendability. The inner bending radius is the significant parameter, indicating the bendability in the bending process. This radius is related to bending moment and the required bend force [30]. Smaller n values will induce a large bending radius, which increases the bending moment and thereby bend force [12]. The larger the bending radius, the smaller is the bend angle [31]. Hence the bend angle decreases with decreasing strain hardening exponent.

Figs. 6(a) and 6(b) depicts the influence of coating thickness on bend force and final bend angle. There is a decrease in bend force and an increase in bend angle with increasing coating thickness. Since zinc has lower shear strength than steel,

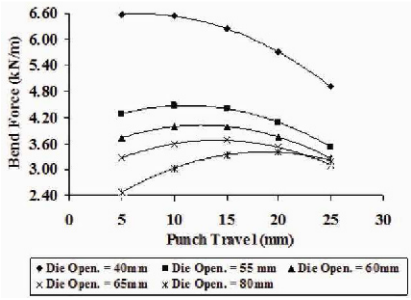

(a)

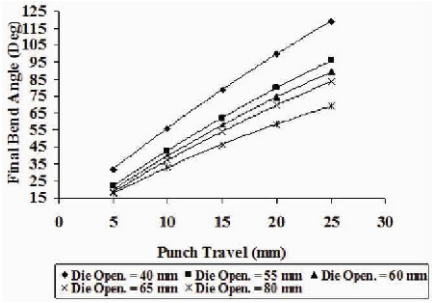

(b)

Fig. 7. Effect of die opening on (a) Bend force; (b) Final bend angle (n = 0.219, t_c = 7μ, R_d = 6.5 mm, R_p = 10 mm, V_p = 0.6 mm/s).

zinc acts as a lubricant [32] when the tool comes in contact with the sheet and reduces the friction. Hence, there is a decreased membrane force [4] and contact pressure over the punch and die profiles [33] which are expected to decrease the bend force and increase the bend angle respectively. The increase in coating thickness reduces friction further [29], resulting in decreasing bend force and increasing bend angle.

The variation of bend force and bend angle with die opening is illustrated in Figs. 7(a) and 7(b). It is noted that the bend force and bend angle increase as the die opening decreases. The lever arm transfers the bend force into bending moment [34]. Since the lever arm is decided by the die opening and the lever arm is getting smaller for smaller die opening, a higher bend force is required to provide the necessary bending moment. It is found that the bend angle is larger for a small die opening. A smaller die opening and a longer punch travel have a similar effect in the bending process [35]. The severity of bending decreases with increasing die opening. Hence, a longer punch travel is required in a larger die opening than smaller one to obtain the same bend angle.

The effect of die radius on bend force and bend angle is shown in Figs. 8(a) and 8(b). It is found that the bend force and bend angle decrease with increasing die radius. An increase in die radius is similar to an increase in die opening in a restricted sense [36] and it results in a large bend angle. Since the point of contact of the tool and support to the sheet are spaced further apart for larger radius, the lever arm increases and a smaller bend force is needed to produce the required bending moment. However, the influence of die radius is not as significant as die opening

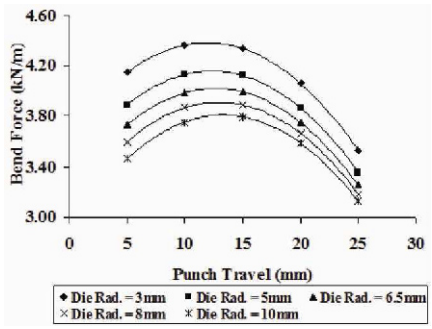

(a)

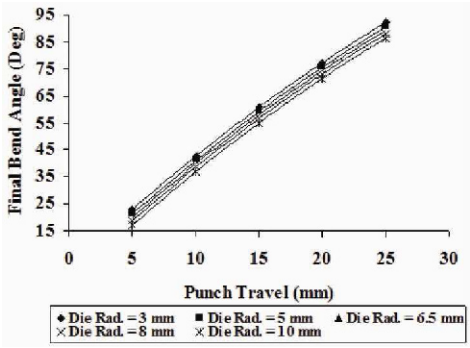

(b)

Fig. 8. Effect of die radius on (a) Bend force; (b) Final bend angle (n = 0.219, t_c = 7μ, W_d = 60 mm , R_p = 10 mm, V_p = 0.6 mm/s).

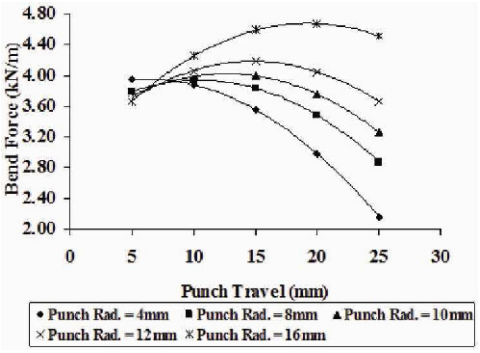

(a)

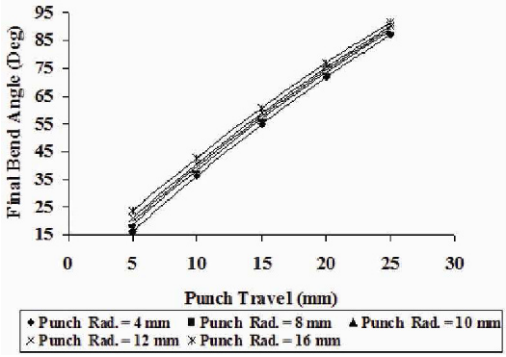

(b)

Fig. 9. Effect of punch radius on (a) Bend force; (b) Final bend angle (n = 0.219, t_c = 7μ, W_d = 60 mm, R_d = 6.5 mm, V_p = 0.6 mm/s).

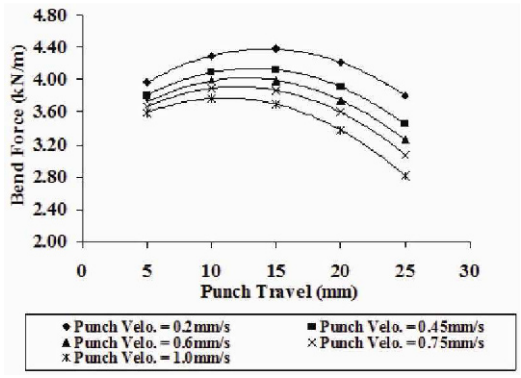

(a)

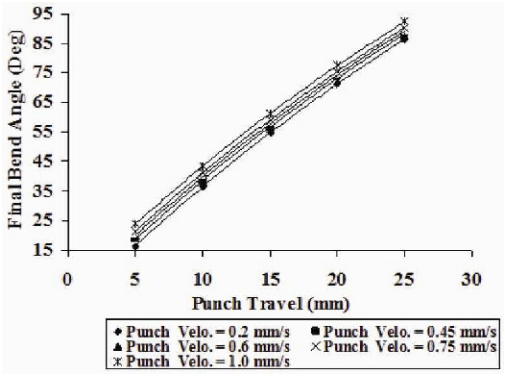

(b)

Fig. 10. Effect of punch velocity on (a) Bend force; (b) Final bend angle (n = 0.219, t_c = 7μ, W_d = 60 mm, R_d = 6.5 mm, R_p = 10 mm).

Figs. 9(a) and 9(b) illustrates the variation of bend force and bend angle for different punch radii. It is observed that bend force and final bend angle increase when the punch radius increases. The reason for increasing bend force is that the magnitude of bend force is governed by the effective stress area over the punch profile which increases with increasing punch radius [3]. The deformation mode of the sheet is either by bending or by shear. The deformation mode is influenced by the effective clearance between the punch and die. Increasing punch radius for a given die opening decreases the effective clearance and shearing takes a dominant part in the deformation of the sheet and this increases the final bend angle. When the punch radius is small , the effective clearance becomes larger and the role of shear is limited [36, 37].

The variation of bend force and bend angle with respect to different punch velocities are plotted in Figs. 10(a) and 10(b). It is found that the bend force is decreased and bend angle is increased with an increase in punch velocity. The reason is, the increase in punch velocity decreases the friction [38], the bend force decreases and bend angle increases accordingly.

3.2 Interaction effect of coating thickness and Punch velocity

Figs. 11(a) and 11(b) show that the bend force decreases

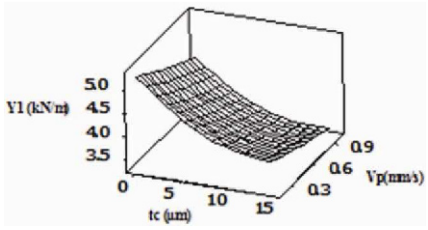

(a)

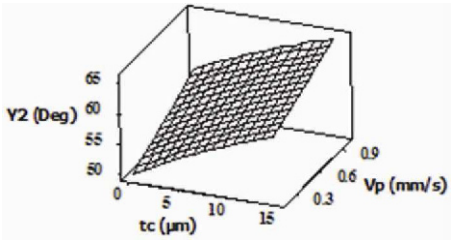

(b)

Fig. 11. Interaction effect of coating thickness and punch velocity on (a) bend force; (b) bend angle.

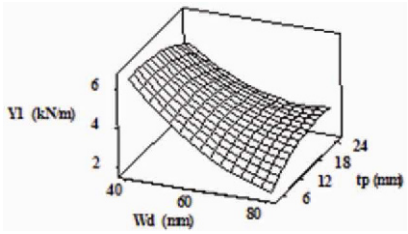

(a)

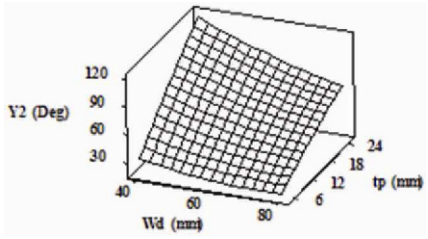

(b)

Fig. 12. Interaction effect of die opening and punch travel on (a) bend force; (b) bend angle.

and bend angle increases with increasing coating thickness and punch velocity. It is because the friction decreases as the coating thickness increases [29] and the punch velocity increases [38]. The reduction in friction causes the bend force to decrease and the bend angle to increase.

3.3 Interaction effect of die opening and punch travel

From Figs. 12(a) and 12(b), it is understood that a larger bend angle is obtained and larger bend force is required when the die opening is narrower and the punch travel is longer. The narrow die opening or longer punch travel increases the severity of bending, which results in a large bend angle. It is evident that the bending moment increases with increasing bend

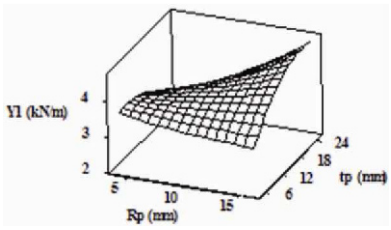

(a)

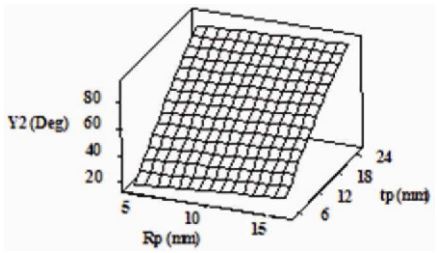

(b)

Fig. 13 Interaction effect of punch radius and punch travel on (a) bend force; (b) bend angle.

angle [31]. As the bend angle increases for a narrower die opening and longer punch travel, the bending moment increases and thereby the bend force also increases

3.4 Interaction effect of punch radius and punch travel

It is noted from the Fig. 13(a) that maximum bend force is reached at shorter punch travel for smaller punch radius and it requires a longer punch travel when the punch radius increases. It is evident from Fig. 13(b) that a larger punch radius or a longer punch travel increases the bend angle.

The bend force is related to the strain level in the bending region, which is determined by the inner radius at air bending [34]. The bend angle is also influenced by the inner radius of curvature underneath the punch. During bending, the process adjusts itself to reduce the bending energy [1]. Hence, initially the sheet bends with larger radius and the sheet radius gradually decreases with punch travel until complete wrap around (inner sheet curvature and punch curvature are same) or till the end of punch travel.

This behavior is determined by effective clearance between the die and the punch. The effective clearance is larger for smaller punch radius, and in this case, a complete wrap around may occur at a shorter punch travel [35]. The increase in punch radius decreases the effective clearance, which causes a change in the course of bend force. In a small punch, with the increase in punch travel, the inner radius continuously decreases, thereby the bend angle increases. In a large punch, the radius decreases with increasing punch travel, but at a certain level the radius does not decrease further. In this case, the deformation of the sheet occurs in the legs of the bend that is drawn into the die opening [35]. Moreover, with increasing punch radius shear plays a major role in the deformation of the sheet [37] and this may be the reason for increasing bend angle.

4. Conclusions

- The adequacy of the developed RSM models were validated statistically from the F-test, normal probability plot of residuals and plot of the residuals versus fitted value.
- The influences of various parameters on bend force and bend angle during air bending are studied based on the developed models. From the study, it is inferred that increasing strain hardening exponent, coating thickness, die opening, die radius, punch velocity decreases the bend force and increasing punch radius, punch travel increases the bend force. Further, the increasing strain hardening exponent, coating thickness, punch radius, punch velocity and punch travel increases the bend angle and increasing die opening and die radius decreases the bend angle.
- The die opening and punch travel are the most significant factors influencing the bend force and bend angle. The effect of the coating is also considerable.
- The results from the developed models are found to have good agreement with the experimental results, and hence the models would be very useful to predict the bend force and final bend angle at various parameter settings within the specified ranges.

Nomenclature

n : Strain hardening exponent
R_d : Die radius
R_p : Punch radius
t_c : Coating thickness
t_p : Punch travel
V_p : Punch velocity
W_d : Die opening
Y_1 : Bend force
Y_2 : Final bend angle

References

[1] L. J. De Vin, Curvature prediction in air bending of metal sheet, *J. Mater. Process. Technol*., 100 (1-3) (2000) 257-261.

[2] H. M. Jiang, X. P. Chen, C. Wu and H. H. Li, Forming characteristics and mechanical parameter sensitivity study on pre-phosphated electro-galvanized sheet steel, *J. Mater. Process. Technol.*, 151 (1-3) (2004) 248-254.

[3] Y. M. Huang and D. K. Leu, Effects of process variables on V-die bending process of steel sheet, *Int. J. Mech. Sci.*, 40 (7) (1998) 631-650.

[4] M. S. Hamouda, F. Abu Khadra, M. M. Hamadan, R. M. Inhemed and E. Mehdi, Springback in v-bending: a finite element approach, *Int. J. Mater. Prod. Technol.*, 21 (1-3) (2004) 124-136.

[5] D. Fei and P. Hodgson, Experimental and numerical studies of springback in air v-bending process for cold rolled TRIP

steels, *Nucl .Eng. Des*., 236 (18) (2006) 1847-1851.

[6] R. Narayanasamy and P. Padmanabhan, Effects of material orientation on air bending of interstitial free steel sheet, *J. manufacturing engineering*, 3 (3) (2008) 163-169.

[7] R. Narayanasamy and P. Padmanabhan, Experimental investigations on effect of process parameters during air bending of interstitial free steel sheet, *J. Manufacturing Engineering*, 3 (4) (2008) 248-255.

[8] M. L. Garcia-Romeu and J. Ciurana, Springback and geometry prediction - Neural networks applied to the air bending process, Huang, D. S., Li, K. and Irwin, G. W. Eds. ICIC 2006, *LNCS 4113*, Springer-Verlag, Berlin Heidelberg, (2006) 470-475.

[9] M. A. Farsi and B. Arezoo, The determination of springback in L bending operation using neural networks, in *Proc. 5th International Advanced Technologies symposium*, Turkey (2009).

[10] Z. Tan, B. Persson and C. Magnusson, An empiric model for controlling springback in V-die bending in sheet metals, *J. Mater. Process. Technol.*, 34 (1-4) (1992) 449-455.

[11] C. Wang, G. Kinzel and T. Atlan, Mathematical modeling of plane-strain bending of sheet and plate, *J. Mater. Process. Technol.*, 39 (3-4) (1993) 279-304.

[12] D. K. Leu, A simplified approach for evaluating bendability and springback in plastic bending of anisotropic sheet metals, *J. Mater. Process. Technol.*, 66 (1-3) (1997) 9-17.

[13] K. L. Elkins and R. H. Sturges, Springback analysis and control in small radius air bending, *J. Manuf. Sci. Eng.*, 121 (4) (1999) 679-688.

[14] W. Y. D. Yuen, A generalised solution for the prediction of springback in laminated strip, *J. Mater. Process. Technol.*, 61 (3) (1996) 254-264.

[15] H. K. Yi, D. W. Kim, C. J. Van Tyne and Y. H. Moon, Analytical prediction of springback based on residual differential strain during sheet metal bending, *Proc. of IMechE, Part C: J. of Mechanical Engineering Science*, 222 (2) (2007) 117-129.

[16] R. H. Myers and D. C. Montgomery, *Response surface methodology: Process and product optimization using designed experiments*, 2nd ed., Wiley, New York, USA (2002).

[17] M. Kleiber, J. Knabel and J. Rojek, Reliability assessment in metal forming operations, *Procs. of the Fifth World Congress on Computational Mechanics (WCCMV)*, Vienna, Austria (2002) 39-40.

[18] T. Ohata, Y. Nakamura, T. Katayama and E. Nakamachi, Development of optimum process design system for sheet fabrication using response surface method, *J. Mater. Process. Technol.*, 143-144 (2003) 667-672.

[19] P. Tiernan, B. Draganescu and M. T. Hillery, Modelling of extrusion force using the surface response method, *Int. J. Adv. Mfg. Technol.*, 27 (1-2) (2005) 48-52.

[20] D. Lepadatu, R. Hambli, A. Kobi and A. Barreau, Optimisation of springback in bending processes using FEM simulation and response surface method, *Int. J.. Adv. Mfg. Technol.*, 27 (1-2) (2005) 40-47.

[21] H. Naceur, Y. Q. Guo and S. Ben-Elechi, Response surface methodology for design of sheet forming parameters to control springback effects, *Comput. Struct.*, 84 (26-27) (2006) 1651-1663.

[22] A. Mkaddem and D. Saidane, Experimental approach and RSM procedure on the examination of springback in wiping-die bending processes, *J. Mater. Process. Technol.*, 189 (1-3) (2007) 325-333.

[23] R. Bahloul, S. Ben-Elechi and A. Potiron, Optimisation of springback predicted by experimental and numerical approach by using response surface methodology, *J. Mater. Process. Technol.*, 173 (1) (2006) 101-110.

[24] D. Vasudevan, R. Srinivasan and P. Padmanabhan**,** Effect of process parameters on springback behaviour during air bending of electrogalvanised steel sheet, *J. Zhejiang Univ.-SCIENCE A*, 12(3) 2011 183-189.

[25] K. T. Chiang, C. C. Chou and N. M. Liu, Application of response surface methodology in describing the thermal performances of a pin-fin type heat sink, *Int. J. Therm. Sci.*, 48 (6) (2009) 1196-1205.

[26] D. C. Montgomery, *Design and analysis of experiments*, 4th ed., John Wiley, New York (1997).

[27] M. Y. Noordin, V. C. Venkatesh, S. Sharif, S. Elting and A. Abdullah, Application of response surface methodology in describing the performance of coated carbide tools when turning AISI 1045 steel, *J. Mater. Process. Technol.*, 145 (1) (2004) 46-58.

[28] L. C. Zhang, G. Lu and S. C. Leong, V-shaped sheet forming by deformable punches, *J. Mater. Process. Technol.*, 63 (1-3) (1997) 134-139.

[29] G. A. Kumar and K. D. Ravi, Formability of galvanized interstitial-free steel sheets, *J. Mater. Process. Technol.*, 172 (2) (2006) 225-237.

[30] N. Asnafi, Springback and fracture in v-die air bending of thick stainless steel sheets, *Mater. Des.*, 21 (3) (2000) 217-236.

[31] M. L. Garcia-Romeu, J. Ciruana and I. Ferrer, Springback determination of sheet metals in air bending process based on an experimental work, *J. Mater. Process. Technol.*, 191 (1-3) (2007) 174-177.

[32] J. Z. Gronostajski, Behaviour of coated steel sheets in forming processes, *J. Mater. Process. Technol.*, 53 (1-2) (1995) 167-176.

[33] J. K. Kim and T. X. Yu, Forming and failure behaviour of coated, laminated and sandwiched sheet metals: a review, *J. Mater. Process. Technol*., 63 (1-3) (1997) 33-42.

[34] R. J. Mentink, D. Lutters, A. H. Streppel and H. J. J. Kals, Determining material properties of sheet metal on a press brake, *J. Mater. Process. Technol.*, 141 (1) (2003) 143-154.

[35] L. J. De Vin, Expecting the unexpected, a must for accurate brake forming, *J. Mater.Process. Technol.*, 117 (1-2) (2001) 244-248.

[36] M. V. Inamdar, P. P. Date and S. V. Sabnis, On the effects

of geometric parameters on springback in sheets of five materials subjected to air vee bending, *J. Mater. Process. Technol.*, 123 (3) (2002) 459-463.

[37] A. H. Streppel, D. Lutters, E. ten Brinke, H. H. Pijlman and H. J. J. Kals, Process modelling for air bending: validation by experiments and simulations, *J. Mater. Process Technol.*, 115 (1) (2001) 76-82.

[38] M. Ramezani, Z. M. Ripin and R. Ahmad, Modelling of kinetic friction in V-bending of ultra-high-strength steel sheets, *Int. J. Adv. Mfg. Technol.*, 46 (1-4) (2010) 101-110.

R. Srinivasan is an Associate Professor in the Department of Mechanical Engineering, Ratnavel Subramaniam College of Engineering and Technology, Dindigul, India. He did both his Bachelor's degree in Mechanical Engineering and Master's degree in Production Engineering in Government College of Technology, Coimbatore. He is presently pursuing his Doctoral degree in Anna University Chennai. His research areas are materials, manufacturing and low cost automation.

D. Vasudevan is Professor and Head, Department of Mechanical Engineering in PSNA College of Engineering and Technology, Dindigul, India. He obtained his Bachelor's degree in Mechanical Engineering from Karnataka University, Dharwad, India, Master's degree in Industrial Engineering from Madurai Kamaraj University, Madurai, India, and Doctorate in Mechanical Engineering from Bharathiar University, Coimbatore, India. His research interests are bio-diesels, manufacturing systems and application of ANN in Mechanical Engineering.

P. Padmanabhan is currently Professor in Department of Mechanical Engineering, VV College of Engineering, Tisaiyanvilai, India. He obtained his Bachelor's degree in Mechanical Engineering from Madurai Kamaraj University and Master's degree in Manufacturing Technology from National Institute of Technology, Tiruchirapalli. His Doctorate is in the area of metal forming from Anna University Chennai. His research interests are manufacturing and process modeling.